RESEARCH ARTICLE

Hybrid Physical Chemical Vapour Deposition (HPCVD) of Superconducting MgB_2 Thin Films on three Dimensional Copper Substrates

Nilanjal Misra[1,2,*], Reza Valizadeh[2], Virendra Kumar[1]

[1]Radiation Technology Development Division, Bhabha Atomic Research Centre, Mumbai 400085, India
[2]ASTEC, Daresbury Laboratory, Science and Technology Facilities Council, Warrington, WA44AD, United Kingdom

*Corresponding author: E-mail: nilanjalm@gmail.com, nilanjal@barc.gov.in

DOI: 10.5185/amlett.2020.111574

The present work reports the design, development and application of a novel Hybrid Physical Chemical Vapour Deposition (HPCVD) technique for depositing MgB_2 thin films, with potential superconductivity, directly on three dimensional (3D) surfaces. A novel solenoid magnetron based set up was used for depositing MgB_2 thin films on 3D surfaces of Cu tube. Mg rod was used as the sputter target and source of Mg while high purity BBr_3 was used as a novel boron precursor, which was injected into the system using Argon as carrier gas. The plasma mediated decomposition of BBr_3 in presence of H_2 gas was followed by chemical reaction between Mg and B atoms to deposit MgB_2 film on the substrate. Samples were characterized by SEM, EDX, XRD and SQUID techniques. SEM-EDX confirmed deposition of a homogeneous, pore free and dense MgB_2 film, while XRD analysis revealed the film to be polycrystalline and multiphasic rather than being purely c-axis oriented. Superconductivity analysis carried out using SQUID measurements indicated a sharp transition with Tc value of 39 K. From the M-H hysteresis loop, the lower critical field Hc_1 and critical current density J_c at 4.2 K were calculated to be 700 Oe and 3.5 x 10^7 A/cm^2, respectively.

Introduction

Since the discovery of superconductivity in binary metallic MgB_2 in the year 2001 [**1**], a significant amount of work has been carried out to fabricate high quality thin films of this new material for fundamental studies and electronic device applications. MgB_2 has found many important applications in power cables, microwave devices and MRI machines. One of its emerging applications is the development of superconducting radiofrequency (SRF) cavities for particle accelerators, made of bulk Copper coated with a layer of MgB_2 thin film, as an attractive alternative to expensive bulk Niobium cavities [**2-4**]. The advantages of such MgB_2 coatings include lower operating costs, improved thermal stability (due to the presence of Cu), low residual resistance, high transition temperature, as well as higher critical fields [**2**]. Since bulk Niobium cavities, which have been in operation for over fifty years, are approaching their theoretical limit, MgB_2 coated cavities show promise as likely substitutes capable of delivering a high-quality factor (Q_0) and high accelerating gradients (E_{acc}) at higher operational temperature. [**5-10**].

MgB_2 has had a considerable impact in the field of superconductivity due to a multitude of reasons. First of all, MgB_2 has a Tc of ~39 K which is the highest superconducting transition temperature among all intermetallic compounds. Secondly, MgB_2 is a phonon-mediated BCS (Bardeen–Cooper–Schrieffer) superconductor, as demonstrated by the isotope effect reported immediately after the first announcement of superconductivity [**11,12**]. Since the Tc is higher than the BCS limit (~30 K), MgB_2 has encouraged researchers to re-examine the old theories and propose alternate mechanisms that involve spin-mediated pairing rather than phonon-mediated pairing, as is the case with high Tc cuprates. The third reason is that MgB_2 has many properties that make it an attractive choice for superconducting applications, such as its suitability in fabricating good Josephson junctions, low anisotropy, fewer material complexities, fewer interface problems and a longer coherence length (ξ ~5 nm).

Consequently, numerous methods have been developed over the years for fabricating MgB_2 coatings, including magnetron sputtering/co-sputtering, chemical vapour deposition (CVD), electrochemical deposition, HPCVD, etc. [**13-15**]. However, most of these methods have certain limitations in terms of film properties such as poor adhesion, non-uniformity, harsh reaction environment, etc. For instance, in the case of physical vapour deposition (PVD), the control of the stoichiometry may be difficult over large areas of accelerator cavities, especially in cases of narrow stoichiometric range. CVD method has been used for deposition of either single or alloys superconducting films, mainly on flat substrates. The deposition rate and the structure of the film depend on the temperature and the reagent concentration. The control of the temperature and gas flow uniformity over the entire cavity surface may be difficult with complex geometries. The main disadvantage of CVD is the high temperature nature of the process and the reduction of existing precursor will only take place at

temperature way above 650 ^{0}C, which can be detrimental to copper cavity structure. Hybridization of PVD and CVD techniques can help eliminate these disadvantages and offer a more efficient approach towards deposition of superconducting thin films. HPCVD of superconducting films can be carried out under relatively milder conditions. Besides, it offers easy control over process parameters through fine tuning of the plasma power, process gas flow rate, substrate to target distance, etc. This method derives its significance from the fact that, if suitably optimized and upscaled for fabrication of SRF cavities, it can significantly cut down on the costs, in addition to enhancing accelerator performance. As an illustrative example, the SRF cavities used in CERN's Large Hadron Collider (LHC) project raise the 450 GeV energy of the particles to 6.5 TeV, a 14-fold amplification of injection energy. A significant amount of expenditure and energy losses during the acceleration process can be conveniently avoided by replacing bulk Nb cavities with the much cheaper but more efficient MgB_2 coated Cu cavities. The demand will increase further with more superconducting cavities being needed in the near future for a potential high energy (HE)-LHC or any of the future circular collider options, which are currently under study [**16**]. With limited number of research groups involved in this field, any notable achievement will be a major boost to CERN's SRF infrastructure, which has become highly relevant due to the growing number of facilities requiring SRF cavities for high intensity and energy upgradation**.** Seong *et. al.,* [**17**] and Withanage *et. al.,* [**18**] have reported using the HPCVD approach to deposit MgB_2 thin films on Al_2O_3 and Copper substrates, respectively. Simultaneously, with doping emerging as a new trend in the area, Pham *et. al.,* have recently deposited ZnO doped MgB_2 thin films with enhanced critical current density [**19**]. On similar lines, Withanage *et. al.,* have also reported on Al ion implanted MgB_2 films for SRF cavity applications [**20**]. However, deposition onto 3D surfaces has been a challenge, which is essential if MgB_2 deposition is to be carried out in actual SRF cavities for particle accelerator applications. Lee *et. al.,* [**21**] is one of the few groups who have managed to deposit MgB_2 inside 3.9 GHz mock cavities. In addition, most of the work has involved using diborane (B_2H_6) as the Boron precursor, which is highly toxic and explosive, making its handling and storage troublesome [**17,18,22**]. Compared to diborane, a boron halide such as boron tribromide (BBr_3), a high vapor pressure liquid, is relatively safer to handle. Moreover, the use of plasma ensures that the precursor molecule decomposition takes place at temperatures much lower than that required to initiate a thermal decomposition for liberation of B atoms in presence of Hydrogen [**23,24**].

In this work, we investigate the practicality and feasibility of using a novel modified HPCVD approach with indigenously developed HPCVD setup to directly deposit superconducting MgB_2 film on 3D surfaces. At the same time the work reports, to the best of our knowledge, the first application of BBr_3 as a Boron source in the deposition of MgB_2 thin films on 3D surfaces for superconductivity applications. This futuristic approach to achieve direct three-dimensional deposition using less toxic, safe and easy to use precursors, i.e., BBr_3, instead of the traditional B_2H_6 gas, is a step towards developing a facile, easily upscalable methodology for new SRF cavity design.

Materials and methods

Materials

High purity Mg target Disc (2.5" diameter, 3 mm thickness, 99.9% purity) and Mg rod (100 cm length, 4.8 mm diameter, 99% purity) were procured from M/s Goodfellow, UK. Mg rods were cut into 30 cm pieces to serve as sputter targets. BBr_3 (99.99% purity. Density=2.64 g.cm^{-3}, molar mass = 250.52 g.mol^{-1}, vapour pressure =7.2 kPa at 20^{0}C) was procured from M/s Sigma Aldrich and used as received. High purity H_2 and Argon gases (purity>99.999%) were procured from Air Liquide, UK and used as received. Copper (Cu) films (0.45 mm thickness) were procured locally and cleaned thoroughly by ultrasonication in acetone bath for ~30 minutes and vacuum dried prior to use. The Cu films were cut into 20 cm x 20 cm pieces and rolled to form tubular substrates of diameter 5 cm. As per the laboratory safety guidelines, all chemical handling and transfers were carried out in a glove box maintained at a N_2 atmosphere with O_2 and H_2O concentrations less than 0.1 ppm.

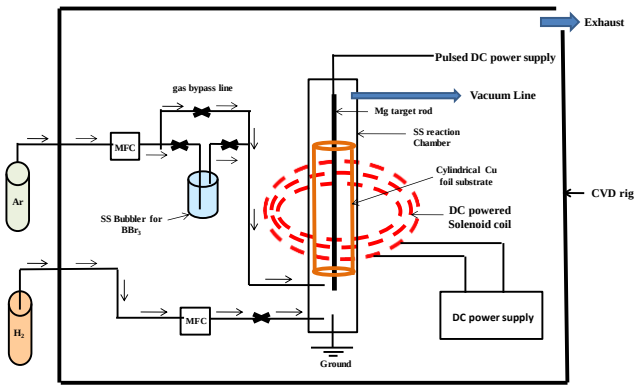

Fig. 1. Schematic representation of Solenoid magnetron-based Hybrid Physical Chemical Vapour Deposition (HPCVD) set up for MgB_2 deposition on 3D surface.

HPCVD set up

For the 3D deposition process, a solenoid based HPCVD set up was indigenously designed and developed (**Fig. 1**). Power supply used was a pulsed power DC source (M/s Advanced Energy Instruments, Pinnacle. 0-1000W range) operated at a frequency of 350 kHz. The Mg sputtering target was confined within a stainless-steel metallic cylinder, which houses the Cu substrate rolled in tubular form and serves as the reaction chamber. The metallic cylinder in turn is surrounded by a solenoid coil powered by a DC power supply (Kenwood PD110-5, 0-110 V) to provide a uniform magnetic field. One gas line is connected from the base of the substrate chamber to introduce H_2 gas to initiate the precursor decomposition reaction within the

plasma. Boron is sourced from high purity BBr_3 contained in a SS bubbler and injected into the reaction chamber using Ar as carrier gas. The flow rate in both gas lines were controlled using gas calibrated mass flow controllers (MKS 1179C, 0-100 sccm). The Ar gas outlet (from the MFC) is connected to the bubbler inlet while the bubbler outlet is connected to the reaction chamber. The line is also provided with a bypass for direct Ar injection during initial plasma generation in absence of the precursor and also for post deposition flushing of the chamber. The precursor flow rate is controlled by the flow rate of carrier gas and also using a leak valve placed between the bubbler and the reaction chamber. The entire set up was pumped down to a pressure of ~6.0 x 10^{-7} mbar via dual stage pumping using an oil rotary pump (Edwards: Atmosphere to 10^{-2} mbar) and a turbomolecular pump (Pfeiffer: 10^{-2} mbar to 10^{-7} mbar) and baked out overnight at 150 ^{o}C, except the SS bubbler, prior to use in order to eliminate any residual moisture and other undesired impurities.

Film deposition process

To initiate the plasma generation, Ar was first injected into the chamber through the bypass at a flow rate of 6-12 sccm while the input power was fixed at 20W (350 kHz). Subsequently, H_2 was slowly introduced into the chamber from the base. The Ar:H_2 gas ratio was optimized at a ratio of 1:15 with flow rates set at 6 and 90 sccm, respectively. The corresponding pressure was observed to be 2.9 x 10^{-3} mbar. The H_2 concentration was kept considerably higher to provide a H_2 rich environment and facilitate decomposition of BBr_3. The SS bubbler was filled with 20 g of BBr_3. The flow rate of BBr_3 into the reaction chamber was regulated by manipulating the flow rate of the carrier gas (final pressure: 2.0 x 10^{-2} mbar). The Mg rod (sputter target) provided a higher Mg overpressure than that required to maintain a Mg/B ratio of 1/2 by generating excess Mg vapours at the applied power of 20W. This was done to compensate for the loss of Mg due to evaporation from the substrate surface during deposition. The solenoid current was maintained at 2.0 Amp to provide a uniform magnetic field for confining the plasma within the reaction zone.

Once a stable plasma was established, BBr_3 was introduced into the chamber by slowly opening the bubbler inlet and outlet while closing the bypass line. The BBr_3 flow into the chamber was controlled using the leak valve. Deposition was carried out for a total duration of 30 minutes wherein the entire precursor was exhausted. At an Ar flow rate of 6 sccm, the precursor (BBr_3) flow rate was estimated to be 60 sccm. The deposited MgB_2 films were subsequently annealed at 800 ^{0}C for 120 minutes, with the final temperature achieved gradually at a heating rate of 10^{0}C/min. The annealing was carried out in a cylindrical heating furnace maintained at a pressure of 1.0 x 10^{-2} mbar.

SEM-EDX analysis

SEM analysis was carried out using a Hitachi table top type SEM instrument (TM3030 plus) operated in the secondary electron mode at 5 kV accelerating voltage. Elemental analysis was carried out using Energy Dispersive X-ray Spectrometer (EDX) with the SDD (silicon drift detector) attached with the Hitachi TM3030 plus SEM. For the elemental analysis, SEM-EDX was operated at 15 kV. The metallic samples were mounted on a stainless-steel stub and loaded into the sample chamber prior to analysis.

XRD analysis

X-ray diffraction (XRD) patterns were collected in grazing incidence on a Rigaku SmartLab system, using CuKα X-rays (λ=1.5406 Å), a 2θ scan range of 10–80° and an ω-offset of 0.7 or 1°. The crystalline phase of the films was determined by matching to literature XRD patterns [**25,26**].

Superconducting Quantum Interference Device (SQUID) magnetometry measurements

DC magnetic susceptibility measurements for MgB_2 bulk powder and film samples were collected using a Magnetic Property Measurement System (MPMS) XL-7 instrument under both Zero Field Cooled (ZFC) and Field Cooled (FC) environments with an applied magnetic field (H) of 100 Oe between 2 K and 300 K. Hysteresis data were collected at 4.2 K in a field range of -4000 Oe to +4000 Oe.

Results and discussion

Although the HPCVD approach has been previously explored for fabricating MgB_2 thin films on three dimensional substrates, most of the experiments have been carried out using B_2H_6 gas as the Boron precursor in a 5:95 % mixture with H_2 (commercially available gas mixture). This, to the best of our knowledge is the first reported work where an attempt has been made to use BBr_3, a liquid with high vapour pressure (7.2 kPa at 20^{0}C) as the alternate B source for HPCVD of MgB_2 films on Cu tubes. Normally, BBr_3 reacts with H_2 to liberate B and HBr at elevated temperatures of ~1300^{0}C [**27**]. However, plasma mediated reactions help initiate BBr_3 decomposition without the need for such high temperatures. In this case, the Ar plasma decomposes BBr_3 in presence of H atoms to liberate B in atomic form, followed by chemical reaction between Mg and B and ultimate deposition of MgB_2 on the substrate [**28**] (eqns. 1,2).

$$2BBr_3 \xrightarrow[\text{Plasma}]{3H_2} 2B + 6HBr \qquad (1)$$

$$Mg + 2B \longrightarrow MgB_2 \qquad (2)$$

As can be seen in **Fig. 2**, the reactions could be visually monitored and witnessed by the change in colour of the plasma plume. The purple Argon plasma plume (Fig. 2(i)) instantaneously changed into a bright whitish plume (Fig. 2(ii)) on introduction of BBr_3 in the reaction chamber. The whitish colour persisted till the exhaustion of the precursor. The MgB_2 film deposited on to Cu substrate was observed to be greyish black in colour (**Fig. 2(iv)**).

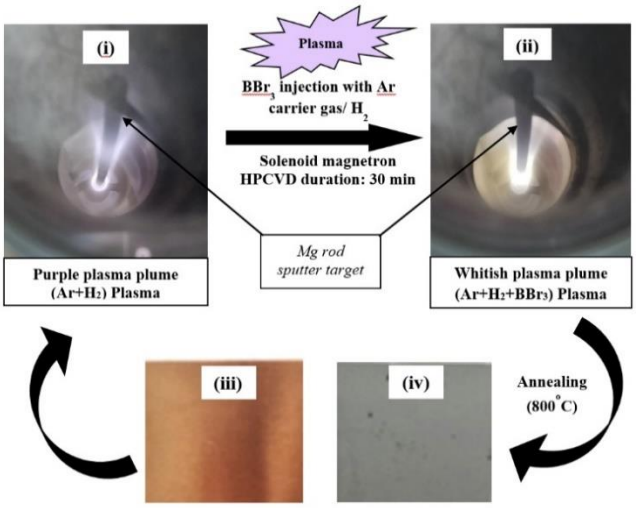

Fig. 2. Images of Plasma plume and samples (i) purple colour of Ar plasma, (ii) whitish colour plasma after introduction of BBr_3, (iii) Pristine Cu film, and (iv) Cu film after deposition of MgB_2.

The results of SEM-EDX analysis of the control Cu film and MgB_2 deposited on 3D configured Cu films are presented in **Fig. 3**. The untreated control Cu film presented a smooth surface morphology (**Fig. 3(a)**). SEM micrograph of the Cu film coated with HPCVD MgB_2 film, presented in **Fig. 3(b)**, revealed the formation of homogeneous, pore free and dense film with the presence of uniformly dispersed spherical particles in the size range of ~500nm (**Fig. 3(c)**). The elemental analyses of the films were carried out by EDX analysis (**Fig. 3(d)**). There was presence of peaks corresponding to Mg, B as well as trace levels of O and Al as impurities in the film. The oxygen is probably introduced by slight surface oxidation on the sample surface whereas presence of trace Al impurities in the commercially procured Cu films could account for the Al peak.

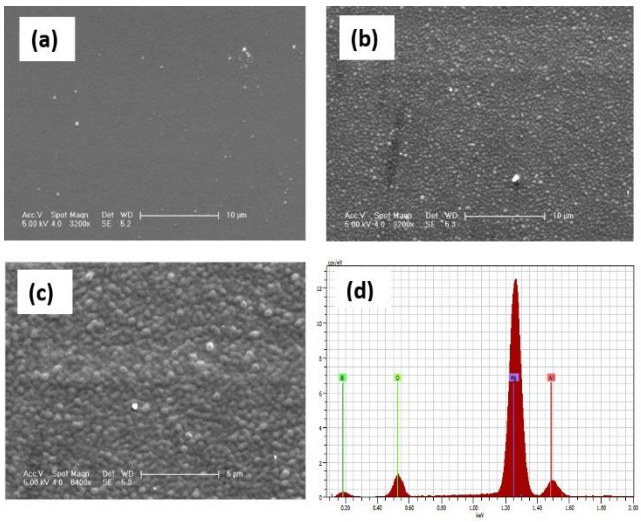

Fig. 3. SEM micrographs (a) Pristine Cu film (Magnification=3200x), (b) Cu film after deposition of MgB_2 (Magnification=3200x), (c) Cu film after deposition of MgB_2 (Magnification=6400x) (d) EDX plot of MgB_2 deposited on Cu film.

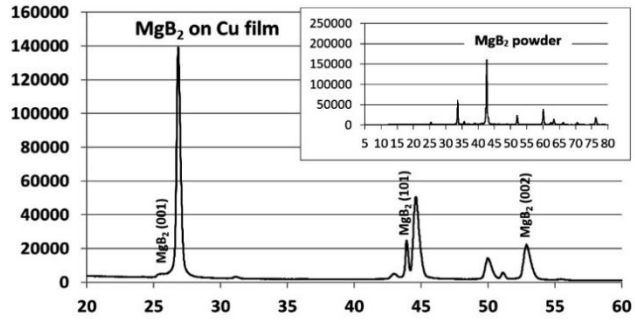

Fig. 4. X-ray diffraction spectra of MgB_2 film deposited on Cu film. Inset: X-ray diffraction spectra of commercial MgB_2 powder.

XRD analysis confirmed the formation of MgB_2 film on the Copper surface. **Fig. 4** shows XRD *θ-2θ* curves in the 2θ range of 20° to 60° for MgB_2 films. Three MgB_2 phase diffraction peaks were observed at 2θ=~25.6°, 43.9° and 53.0° corresponding to (001) (101) and (002) planes, respectively, implying that the MgB_2 has a polycrystalline structure rather than being purely c-axis oriented. In addition, diffraction peaks (222) due to $MgCu_2$ were also observed at 44.6^0, which was consistent with a previous report by Kikuchi *et. al.*, [**25**]. It has also been reported that MgB_4 (220) and MgO (200) crystal peak (formed due to the high sensitivity of Mg towards oxidation) [**29,30**] are occasionally observed as impurities in addition to $MgCu_2$. However, since these peaks can overlap with that of $MgCu_2$, the presence of neither of these impurities could be conclusively confirmed in our sample. In comparison, commercial MgB_2 powder showed distinct diffraction peaks at 2θ = 33.6°, 42.6°, 52.1°, 60.1°, 62.7° and 76.4^0 corresponding to (100), (101), (002), (110) (102) and (201) planes, respectively (**Fig. 4 inset**).

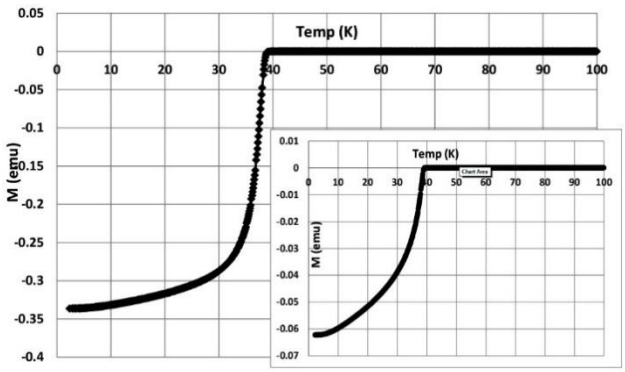

Fig. 5. Zero-field-cooled (ZFC) magnetic moments vs. temperature curve of MgB_2 film deposited on Cu measured in 100 Oe DC magnetic field. Inset: Zero-field-cooled (ZFC) magnetic moments vs. temperature curve of commercial MgB_2 powder measured in 100 Oe DC magnetic field.

SQUID magnetometric measurements were carried out to determine the DC superconducting properties of the MgB_2 thin films. **Fig. 5** and **Fig. 5 inset** show zero-field-cooled (ZFC) magnetic moment vs. temperature curve of MgB_2 measured in a 100 Oe DC magnetic field for HPCVD MgB_2 film and commercial MgB_2 powder, respectively. The commercial MgB_2 sample as well as MgB_2 deposited in

3D configuration displayed a smooth superconducting transition at ~39 K, which was in close agreement with the theoretical value of 39.2 K. This indicated that the stoichiometry of the deposited film matched with the desired Mg/B ratio of ½ and the film deposited was defect free and homogeneous, which resulted in the excellent superconducting transition.

Fig. 6 shows magnetic moment vs. magnetic field (M-H) hysteresis loop for MgB_2 film, measured in a perpendicular field between 4000 Oe and -4000 Oe at 4.2 K. The slight discontinuity in the hysteresis plot may be due to the presence of trace impurities and higher stoichiometries of MgB_x formed along with MgB_2. From the point where the negative part of the M(H) dependence (diamagnetic Meissner phase) starts to deviate from linear behaviour, the Hc_1 value (the point where the magnetic field begins penetrating into the sample) was determined to be ~700 Oe at 4.2 K. It has been reported that due to the geometry barrier, thin film MgB_2 would have a higher Hc_1 than the bulk material (270-480 Oe). Moreover, the Hc_1 of MgB_2 thin films increase with decreasing film thickness. In case of polycrystalline MgB_2 films, the reported Hc_1 values are 520 Oe at 5 K for a 300 nm film and 1520 Oe for a 100 nm film [**31,32**]. Therefore, the observed Hc_1 of ~700 Oe at 4.2 K for a film thickness of ~260 nm can be correlated to this observation.

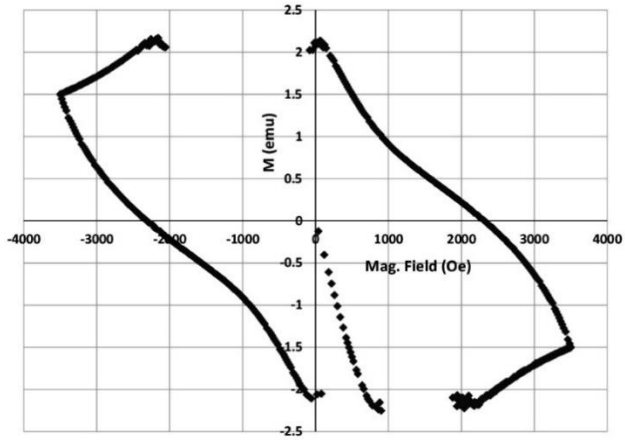

Fig. 6. Magnetic moment vs. Magnetic field (M-H) hysteresis loop for MgB_2 film deposited on Cu (3D) measured in a perpendicular field between +4000 Oe and -4000 Oe at 4.2 K.

The critical current density, J_c ($A.cm^{-2}$) is another important parameter that decides the efficiency of a superconducting material. It is the upper threshold of current density that a material can carry without losing its superconducting properties. For many practical applications of superconductors, the ability to carry high currents in the presence of magnetic fields is very important. The Bean model [**33**] was used to calculate J_c from the M-H hysteresis loop, using equation (3)

$$J_c\,(A.cm^{-2}) = 30\,\Delta M/a \qquad (3)$$

where, 2a= sample film thickness (cm)
$\Delta M=\Delta m/V$, Δm = width of hysteresis loop (emu)
V=volume of sample film (cm^3)

Using this equation, the J_c for polycrystalline MgB_2 thin film was calculated to 3.5 x 10^7 $A.cm^{-2}$ at zero applied magnetic field and 4.2 K, which was in close agreement with the reported values at zero field for HPCVD deposited MgB_2 films on Cu disc surfaces [**18**]. This indicated that the new HPCVD process developed in this work for deposition of MgB_2 film on Cu tubes yielded results comparable with the available literature and is desirable for SRF cavity applications.

Conclusion

A unique solenoid magnetron based HPCVD approach was designed and employed for direct thin film deposition on 3D substrates. Using this technique, MgB_2 was deposited on 3D copper surfaces (tubes), wherein the possibility of using BBr_3 as a new Boron precursor source, instead of B_2H_6, was also investigated and demonstrated to be feasible. The present investigations revealed successful deposition of a superconducting film of polycrystalline MgB_2 on 3D Cu surfaces with a superconducting critical transition Tc = 39 K and critical current density J_c = 3.5 x 10^7 $A.cm^{-2}$ at 4.2 K, which were in agreement with the theoretical and literature values. The possibility of directly depositing HPCVD MgB_2 films on 3D surfaces has potential applications in designing SRF cavities for particle accelerators through deposition of MgB_2 layers on the inner surface of Copper cavities.

Acknowledgement

This work was conducted under the aegis of the Science and Technology Facilities Council (STFC). Nilanjal Misra would also like to thank ASTEC, STFC for the support and the Rutherford International Postdoctoral Fellowship scheme for funding this work. Authors would like to thank Dr. Gavin Stenning, RAL, STFC for the SQUID analysis and Prof. James Bradley, University of Liverpool for his technical guidance.

Keywords

Hybrid physical chemical vapour deposition, BBr_3, MgB_2 film, superconductivity.

Received: 23 May 2020
Revised: 05 August 2020
Accepted: 12 August 2020

References

1. Nagamatsu, J.; Nakagawa, N.; Muranaka, T.; Zenitani, Y.; Akimitsu, J.; Nature, **2001**, *410*, 63.
2. Padamsee, H.; Knobloch, J.; Hays, T.; RF Superconductivity: Science, Technology and Applications. Wiley-VCH Verlag GmbH & Co. KGaA, Weinheim, Germany, **2009**.
3. Kneisel, P.; Myneni, G. R.; Ciovati, G.; Proc. Particle Accelerator Conf., **2005**, 3991.
4. Finnemor, D. K.; Stromberg, T. F.; Swenson, C. A.; *Phys. Rev.*, **1966**, *149*, 231.
5. James, C.; Krishnan, M.; Bures, B.; Tajima, T.; Civale, L.; Edwards R.; Spradlin, J.; Inoue, H.; *IEEE Trans. Appl. Supercond.*, **2013**, *23*, 1.
6. Collings, E.W.; Sumption, M.; Tajima, D.T.; *Supercond. Sci. Technol.*, **2004**, *17*, 595.
7. Cifariello, G.; Aurino, M.; Di Gennaro, E.; Lamura, G.; Andreone, A.; Orgiani, P.; Xi, X. X.; Villegier, J. C.; *Appl. Phys. Lett.*, **2006**, *88*, 1.
8. Buzea, C.; Yamashita, T.; *Supercond. Sci. Technol.*, **2001**, *14*, 115.
9. Larbalestier, D.; Gurevich, A.; Feldmann, D. M.; Polyanskii, A.; *Nature*, **2001**, *414*, 368.

10. Catelani, G.; Sethna, J. P.; *Phys. Rev. B.*, **2008**, *78*, 1.
11. Bud'ko, S. L., Lapertot, G.; Petrovic, C.; Cunningham, C. E.; Anderson, N.; Canfield, P. C.; *Phys. Rev. Lett.*, **2001**, *86*, 1877.
12. Hinks, D. G.; Claus, H.; Jorgensen, J. D.; *Nature*, **2001**, *411*, 457.
13. Schneider, R.; Geerk. J.; Linker, G.; Ratzel, F.; Zaitsev, A. G.; Obst, B.; *Physica C*, **2005**, *423*, 89.
14. Xi, X.X.; Pogrebnyakov, A.V.; Xu, S.Y.; Chen, K.; Cui, Y.; Maertz, E.C.; Zhuang, C.G.; Li, Q.; Lamborn, D. R.; Redwing, J. M.; Liu, Z. K.; Soukiassian, A.; Schlom, D. G.; Weng, X. J.; Dickey, E. C.; Chen, Y. B.; Tian, W.; Pan, X. Q.; Cybart, S. A.; Dynes, R. C.; *Physica C: Supercond.*, **2007**, *456*, 22.
15. Jadhav, A. B.; Pawar, S. H.; *Supercond. Sci. Technol.*, **2003**, *16*, 752.
16. Frank, G.; *IEEE Trans. Appl. Supercond.*, **2018**, *28*, 3500205.
17. Seong, W. K.; Huh, J. Y.; Jung, S. G.; Kang W. N.; Lee, H. S.; Choi, E. M.; Lee, S. I.; *J. Kor. Phys. Soc.*, **2007**, *51*, 174.
18. Withanage, W. K.; Xi, X. X.; Nassiri, A.; Lee, N.; Wolak, M. A.; Tan, T.; Welander, P. B.; Franzi, M.; Tantawi, S.; Kustom, R. L.; *Supercond. Sci. Technol.*, **2017**, *30*, 045001.
19. Pham, D.; Ngoc, H. V.; Jung, S. G.; Kang, D. J.; Kang, W. N.; *Curr. Appl. Phys.*, **2018**, *18*, 762.
20. Withanage, W. K.; Kasaei, L.; Qin, F.; Xi. X. X.; *IEEE Trans. Appl. Supercond.*, **2019**, *29*, 7500204.
21. Lee, N.; Withanage, W. K.; Tan, T.; Wolak, M. A.; Nassiri, A.; Xi, X.; *IEEE Trans. Appl. Supercond.*, **2017**, *27*, Art. No. 3500304.
22. Wang, S. F; Zhu, Y. B; Liu, Z.; Zhou, Y. L.; Zhang, Q.; Chen, Z. H.; Lu, H. B.; Yang, G. Z.; *Chin. Phys. Let.*, **2003,** *20*, 1356.
23. Imam, M.; Souqui, L.; Herritsch, J.; Stegmüller, A.; Höglund, C.; Schmidt, S.; Hall-Wilton, R.; Högberg, H.; Birch, J.; Tonner, R.; Pedersen, H. J.; *Phys. Chem. C*, **2017**, *121*, 26465.
24. Cholet, V.; Herbin, R.; Vandenbulcke, L.; *Thin Sol. Films*, **1990**, *188*, 143.
25. Kikuchi, A.; Yoshida, Y.; Iijima, Y.; Banno, N.; Takeuchi, T.; Inoue, K.; *Supercond. Sci. Technol.*, **2004**, *17*, 781.
26. Liang, G.; Tang, Z.; Fang, H.; Katz, D.; Salama, K.; *J. Alloys Comp.*, **2006**, *422*, 73.
27. Bykova, J. S.; Lima, M. D.; Haines, C. S.; Tolly, D.; Salamon, M. B.; Baughman, R. H.; Zakhidov, A. A.; *Adv. Mater.*, **2014**, *26*, 7510.
28. Ruello, Y.; Cadier, B.; US Patent FR2763327A1, **1997**
29. Savaskan, B.; Ozturk, K.; Celik, S.; Yanmaz, E.; *J. Phys.: Conference Series*, **2009**, *153*, 012023.
30. Rogado, N.; Hayward, M. A.; Regan, K. A.; *J. Appl. Phys.*, **2002**, *91*, 274.
31. Beringer, D. B.; TFSRF New Ideas Workshop, **2012.**
32. Xi, X.; Temple University of the Commonwealth System Final Technical Report, **2017.**
33. Bean, C. P.; *Rev. Mod. Phys.*, **1964**, *36*, 31.